ACSNANO

www.acsnano.org

ARTICLE

Trion-Mediated Förster Resonance Energy Transfer and Optical Gating Effect in WS_2/hBN/$MoSe_2$ Heterojunction

Zehua Hu, Pedro Ludwig Hernández-Martínez, Xue Liu, Mohamed-Raouf Amara, Weijie Zhao, Kenji Watanabe, Takashi Taniguchi, Hilmi Volkan Demir, and Qihua Xiong*

Cite This: *ACS Nano* 2020, 14, 13470−13477

Read Online

ACCESS | Metrics & More | Article Recommendations | Supporting Information

ABSTRACT: van der Waals two-dimensional layered heterostructures have recently emerged as a platform, where the interlayer couplings give rise to interesting physics and multifunctionalities in optoelectronics. Such couplings can be rationally controlled by dielectric, separation, and stacking angles, which affect the overall charge or energy-transfer processes, and emergent potential landscape for twistronics. Herein, we report the efficient Förster resonance energy transfer (FRET) in WS_2/hBN/$MoSe_2$ heterostructure, probed by both steady-state and time-resolved optical spectroscopy. We clarified the evolution behavior of the electron−hole pairs and free electrons from the trions, that is, ∼59.9% of the electron−hole pairs could transfer into $MoSe_2$ by FRET channels (∼38 ps) while the free electrons accumulate at the WS_2/hBN interface to photogate $MoSe_2$. This study presents a clear picture of the FRET process in two-dimensional transition-metal dichalcogenides' heterojunctions, which establishes the scientific foundation for developing the related heterojunction optoelectronic devices.

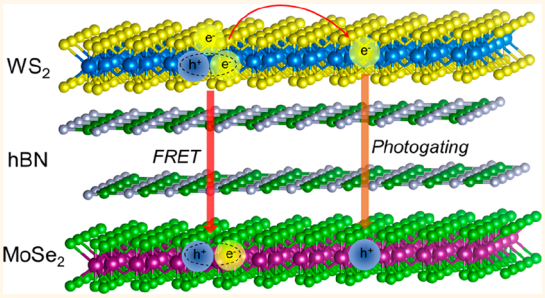

KEYWORDS: *2D materials, transition metal dichalcogenides, trion, van der Waals heterostructure, Förster resonance energy transfer, photogating, optical spectroscopy*

Energy transfer refers to the nonradiative transfer of an electronic excitation from a donor to an acceptor. This process avoids the emission and reabsorption events, thus possessing a high energy-conversion efficiency.[1] Energy transfer can be divided into Dexter and Förster type, whereas the former is based on electron exchange and thus only works in the close proximity (<1 nm); while the latter depends on dipole−dipole coupling and works in a relatively long distance (r) with a $1/r^6$ dependence in the molecular dye system.[2,3] During the past three decades, Förster resonance energy transfer (FRET) has been intensively studied for various important optoelectronic applications including solar cell,[4] light-emitting diode,[5] and laser.[6] Such applications in optoelectronics are highly compatible with recently emerged two-dimensional (2D) van der Waals materials. Due to the reduced dimension and strong confinement in the 2D limit, the dipole−dipole coupling strength is proportional to $1/r^4$, rather than $1/r^6$ in 3D confinement, enabling a stronger interaction strength and more pronounced long-range characteristics.[7,8]

2D materials such as graphene, hexagonal boron nitride (h-BN), and transition metal dichalcogenides (TMDs) offer a platform to study fundamental physics in a single atomic layer limit.[9,10] Monolayer TMDs hold high stability and sizable direct bandgap covering from the visible to near-infrared spectrum. Because of the reduced dielectric screening effect, monolayer TMDs feature strong excitonic emission even at room temperature with a binding energy of several hundred meV.[11] Many-body effect of the excitonic species is strong and highly sensitive to the doping level, allowing the characterization and manipulation of trions or even biexcitons.[12,13] Inversion symmetry breaking and strong spin−orbit coupling enable more exciting physics, including valleytronics and spin-forbidden dark states.[14,15] Since monolayer TMD heterojunctions usually form type II band alignment, optically excited electrons and holes are readily separated and then accumulate in the opposite monolayers. The pump−probe method has proven that such charge transfer process in the heterostructure is ultrafast (∼100 fs).[16−21] The appropriate material

Received: July 1, 2020
Accepted: September 23, 2020
Published: September 23, 2020

https://dx.doi.org/10.1021/acsnano.0c05447
ACS Nano 2020, 14, 13470−13477

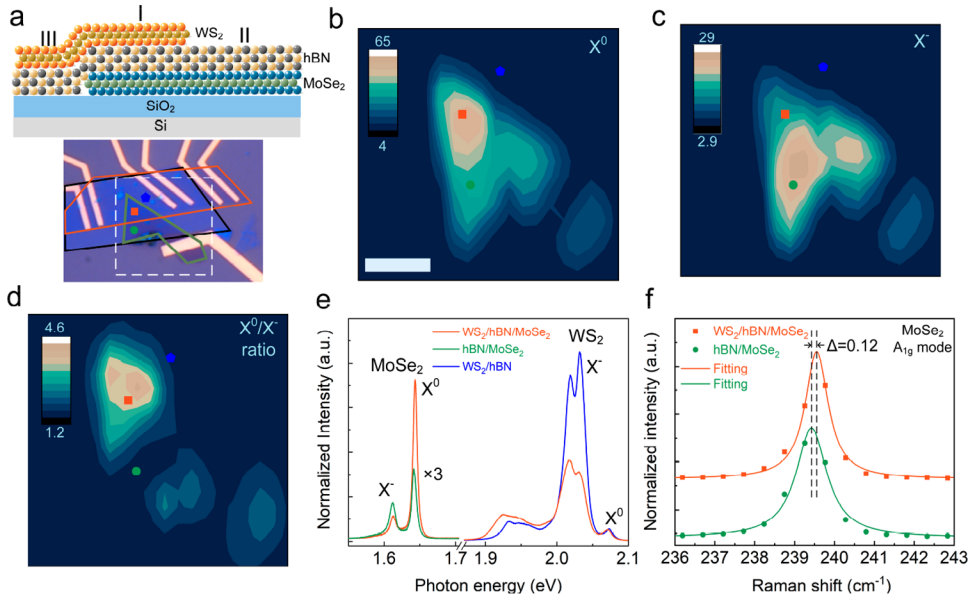

Figure 1. Sample image and optical spectroscopy of the monolayer WS_2/few-layer hBN/monolayer $MoSe_2$ heterojunction excited by 532 nm laser. Orange, black, and green sketch denote WS_2, hBN and $MoSe_2$, respectively. White dashed square indicates the mapping area. Same color indication holds along this paper. a Device structure and optical image. (b–d) PL mapping of $MoSe_2$ X^0(b), X^- (c) and X^0/X^- ratio (d) over the white dash square indicated in (a). (e, f) PL (e) and Raman (f) spectra in the corresponding sample position. The scale bar in (b) is 5 μm.

combination and careful stacking (e.g., $MoSe_2$ and WSe_2) can form a strong interlayer exciton with long lifetime and novel valleytronic properties.[22,23] Besides charge transfer, energy transfer is another important interaction between semiconducting emitters, which are widely studied in quantum dots and organic molecules but much less in 2D material heterojunctions.[24−30] Recently, by performing photoluminescence excitation (PLE) spectroscopy, FRET has been demonstrated in type II $MoSe_2/WS_2$ heterojunction.[31] On the contrary, energy transfer at the $MoTe_2/WSe_2$ interface is demonstrated to be Dexter type by pump−probe method; thus, both direct and indirect exciton from the donor could transfer and contribute to the acceptor emission.[32] Although FRET has been achieved in 2D material heterojunctions, it is simply attributed to a dipole−dipole coupling between excitons.[31,33] However, due to the reduced Coulomb screening effect and high intrinsic doping, 2D TMDs feature diverse emission species, including exciton, trion and even biexciton emission. The population and lifetime of different excitonic species are quite different; thus, one needs to be extremely careful when dealing with the dynamics in 2D TMD heterojunctions.[12,34,35]

Here, we experimentally investigate the energy transfer process in WS_2/hBN/$MoSe_2$ heterojunction. By 532 nm (above WS_2 bandgap) excited photoluminescence (PL) mapping, we observe an enhancement of $MoSe_2$ exciton (X^0) emission, accompanied by the quenching of WS_2 trion (X^-) emission. Such energy transfer occurs via a 3 nm hBN spacer, implying a clear signature of FRET. In combination with the shortening of WS_2 X^- PL lifetime, our study unambiguously reveals that FRET happens between X^- of WS_2 and X^0 of $MoSe_2$, that is, trion-exciton coupling owing to the strong coupling strength and a long intrinsic lifetime of X^-, rather than the direct exciton−exciton coupling proposed in literature.[31,33]

RESULTS AND DISCUSSION

All the heterojunctions are fabricated with standard stamp-assisted dry transfer method in the nitrogen-filled glovebox to minimize the influence from trapped moisture. After transfer, 5/60 nm chromium/gold electrodes are patterned by standard electron beam lithography process, followed by a high vacuum (10^{-6} mbar) annealing at 200 °C for 2 h to enhance the interlayer coupling. All the optical spectroscopies presented in this paper are taken at 80 K in a liquid-nitrogen-cooled cryostat unless otherwise stated.

Figure 1a shows the schematic structure and the optical image of the typical device. Here, monolayer WS_2, ∼3 nm thick hBN, and monolayer $MoSe_2$ are stacked layer by layer to form a heterojunction with distinct regions composed of (I) WS_2/hBN/$MoSe_2$ (orange square in the sample image); (II) hBN/$MoSe_2$ (green circle); and (III) WS_2/hBN. Therefore, the influence of WS_2 on the optical properties of $MoSe_2$ (or vice versa) can be qualitatively and quantitatively compared. Figure 1b–d illustrates the PL mapping data for $MoSe_2$ X^0, X^- and X^0/X^- ratio excited by a 532 nm continuous-wave (CW) laser from the white dashed square in the bottom of Figure 1a. Compared to the case of $MoSe_2$ in region II, the $MoSe_2$ X^0 emission in the region I is enhanced by a factor of ∼2.1 while the X^- emission is decreased by a factor of ∼2/3 (Figure 1b,c), leading to a much higher $MoSe_2$ X^0/X^- ratio (Figure 1d), as reflected in the extracted PL spectra (Figure 1e). The changes of peak position and full width at half-maximum (1.64 eV and 7 meV for X^0; 1.61 eV and 11 meV for X^-) are negligible due to nearly identical dielectric environment ($MoSe_2$ is sandwiched between SiO_2 and hBN). The enhancement of X^0 emission is attributed to the FRET from WS_2 as detailed later, while the X^- emission quenching results from the optical gating effect (p-doping) induced by the electron accumulation at the WS_2/hBN interface.

The optical gating scenario was confirmed by the Raman spectroscopy at the same position, which shows a small redshift

https://dx.doi.org/10.1021/acsnano.0c05447
ACS Nano 2020, 14, 13470−13477

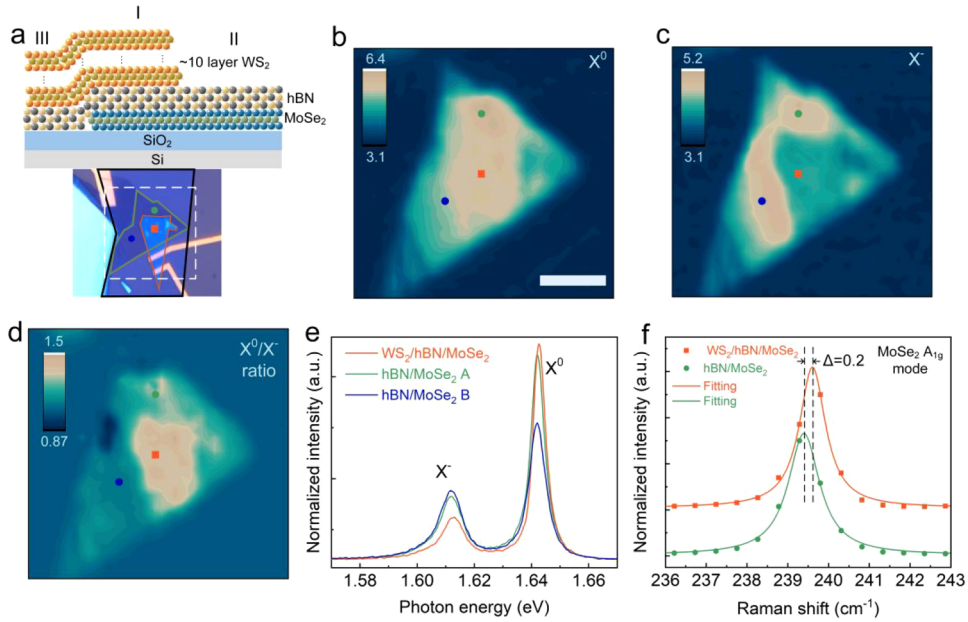

Figure 2. Sample image and optical spectroscopy of the multilayer WS_2/few-layer hBN/monolayer $MoSe_2$ heterojunction excited by 532 nm laser. a Device structure and optical image. (b–d) PL mapping of $MoSe_2$ X^0 (b), X^- (c), and X^0/X^- ratio (d) over the white dash square indicated in (a). (e, f) PL (e) and Raman (f) spectra in the corresponding sample position. The scale bar in (b) is 5 μm.

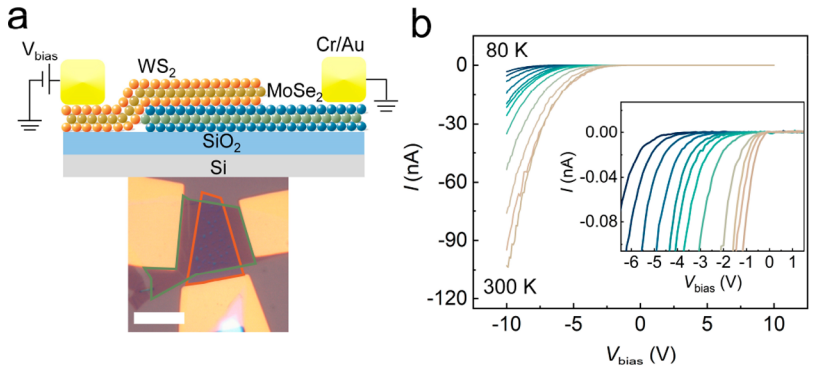

Figure 3. Electrical performance of the monolayer WS_2/monolayer $MoSe_2$ device. (a) The heterojunction device image and structure. The scale bar is 5 μm. (b) Linear scale *I*–*V* performance from 80 to 300 K with an increment of 20 K. Inset: the zoom-in image of the low bias part.

of $MoSe_2$ A_{1g} mode by ~0.12 cm^{-1} in the region I (Figure 1f, full-scale spectra is shown in Supplementary Figure 3a). As previously shown in the literature, the A_{1g} mode of TMDs is sensitive to the doping level due to the strong electron–phonon coupling.[36] Hence, the small redshift here is the direct evidence of weak p-doping.[36] For WS_2, the PL is dominated by X^- emission. The stacking of hBN/$MoSe_2$ quenched the WS_2 X^- emission intensity by almost half, suggesting the exciton energy transfer from WS_2 X^- to $MoSe_2$ X^0 (Figure 1e).

Then, the excitation wavelength was tuned to 671 nm (i.e., below WS_2 bandgap excitation, Supplementary Figures 1, 4). All the $MoSe_2$ X^0, X^-, and X^0/X^- ratio are quite homogeneous among the whole sample, indicating the absence of optical gating, charge, or energy transfer (Supplementary Figure 4b–e). The absent interlayer interaction leads to the negligible peak shift of $MoSe_2$ A_{1g} mode as expected (Supplementary Figure 4f). This result confirms the FRET and optical gating scenery with 532 nm excitation from another perspective. Meantime, the interference effect from the SiO_2 substrate is ruled out by repeating the result on a transparent sapphire substrate, as detailed in Supplementary Figure 5.

For comparison, we fabricated another typical heterostructure device consisting of a multilayer WS_2 (~10 nm), hBN dielectric layer, and monolayer $MoSe_2$, as presented in Figure 2a. As seen from the spectroscopy mapping excited by 532 nm laser, the $MoSe_2$ X^0 is quite uniform in the whole sample area, indicating no energy transfer (Figure 2b). The absence of FRET results from the negligible interaction between the indirect exciton in multilayer WS_2 and the direct exciton in monolayer $MoSe_2$.[32,37] The significant difference from the FRET scenery in Figure 1 confirms the origin of the FRET process (i.e., from the direct dipole–dipole coupling). Meanwhile, the $MoSe_2$ X^- emission is quenched by a factor of ~3/5 at the region I, in agreement with the photogating scenery (i.e., photogenerated electrons accumulate at the WS_2/hBN interface, Figure 2c,e). The redshift of $MoSe_2$ A_{1g} mode is 0.2 cm^{-1} in the region I, slightly larger than 0.12 cm^{-1} in the monolayer case in Figure 1, indicating the slightly stronger p-doping effect, which results from the higher optical absorption

https://dx.doi.org/10.1021/acsnano.0c05447
ACS Nano 2020, 14, 13470–13477

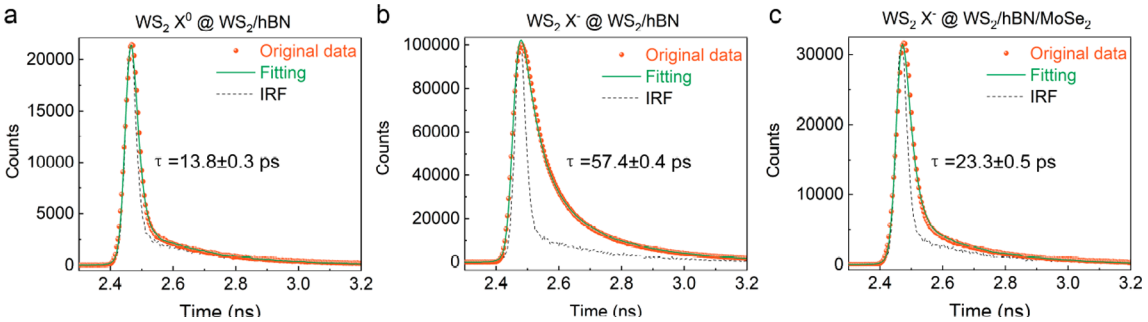

Figure 4. Time-resolved PL of WS_2 measured at 80 K. (a) X^0 at WS_2/hBN, (b) X^- at WS_2/hBN, and (c) X^- at WS_2/hBN/$MoSe_2$. The IRF is provided as a reference.

and larger density of states in multilayer than monolayer WS_2 (Figure 2f). Similarly, the excitation wavelength was then tuned to 671 nm, which shows a negligible change of $MoSe_2$ X^0 emission due to the absence of FRET, as expected (Supplementary Figure 6).

To understand the band alignment, which dominates the interlayer interactions in the heterojunction, we performed the electrical $I-V$ measurement, as shown in Figure 3. The tunneling heterojunctions in the region I of Figures 1 and 2 cannot operate because of the poor conductance of TMD monolayers and the insulating hBN layer. Hence, we use the heterojunctions of monolayer WS_2/monolayer $MoSe_2$ and multilayer WS_2/few-layer hBN/multilayer $MoSe_2$ instead (Figure 3, Supplementary Figure 8). In Figure 3a, the WS_2 and $MoSe_2$ layers are biased and grounded, respectively. The linear scale $I-V$ curve at different temperatures shows the typical diode characteristics, with a negative turn-on voltage and rectification ratio of $\sim 10^5$ at room temperature (Figure 3b). Since the majority carrier in both WS_2 and $MoSe_2$ are electrons, the negative turn-on voltage is an indicator that the conduction band (CB) of WS_2 lies above $MoSe_2$, in agreement with the band alignment calculated by Heyd–Scuseria–Ernzerhof (HSE06) method.[38] This result is also supported by the negative turn-on voltage in the $I-V$ curve of the multilayer WS_2/few-layer hBN/multilayer $MoSe_2$ heterojunction (Supplementary Figure 8b). With increasing temperature, the current increases while the turn-on voltage decreases monotonously, implying the thermionic-emission-dominated transport mechanism (Supplementary Figure 9).

The dynamic processes in the heterojunction were evaluated by the time-resolved PL (spectral resolution ~2 nm), as plotted in Figure 4. The lifetime of WS_2 X^0 (2.07 eV) on hBN, X^- (2.03 eV) on hBN and hBN/$MoSe_2$ are measured to be 13.8 ± 0.3, 57.4 ± 0.4, and 23.3 ± 0.5 ps, respectively, after deconvolution and fitting with a single exponential decay function $I = I_0 e^{-t/\tau}$ (Figure 4a–c). It should be emphasized that the radiative recombination of exciton in the 2D system is very fast due to the small exciton Bohr radius and the large exciton optical oscillator strength, that is, in subpicosecond to picosecond time scale, as demonstrated in numerous theoretical and pump–probe investigations.[34,35,39−41] The WS_2 X^0 lifetime approaches the temporal resolution of our testing system, as learned from the comparison between the experimental data and the instrument response function (IRF) curve (Figure 4a). Such a short lifetime indicates that WS_2 X^0 tends to recombine radiatively rather than transfer to the acceptor. However, it should be noted that the WS_2 PL is dominated by X^- emission, which forms within ~2 ps after exciton formation (Figure 1e).[42] The radiative lifetime of WS_2 X^- (57.4 ± 0.4 ps) is much longer than that of the X^0 due to the difficulty for the electron dissociated from the X^- to find an unoccupied state in the band.[34,39] As a result, in the heterojunction, the electron–hole pair from X^- in WS_2 tends to transfer into $MoSe_2$ and recombine by emitting a X^0 photon. We can calculate the FRET rate ($1/\tau_{FRET}$) and efficiency (η_{FRET}) according to the formula, $1/\tau_{FRET} = 1/\tau_{het} - 1/\tau_{donor}$ and $\eta_{FRET} = 1 - \tau_{het}/\tau_{donor}$, in which τ_{donor} and τ_{het} denote the 1/e lifetime of the WS_2 X^- on hBN and hBN/$MoSe_2$, respectively.[26,43] The corresponding value τ_{FRET} is ~38.4 ps and η_{FRET} is 59.9%, matching well with the ~50% attenuation of the WS_2 X^- intensity as indicated by the steady-state PL spectra (Figure 1e). During the FRET process, the electrons dissociated from the X^- accumulate at the WS_2/hBN interface, leading to the optical gating effect as aforementioned.

Besides, we used COMSOL to numerically simulate the FRET rate in monolayer WS_2/few-layer hBN/monolayer $MoSe_2$ heterojunction. We first check the exciton FRET dynamics by placing a dipole inside the WS_2 monolayer with the $MoSe_2$ monolayer as the absorber medium. The model and the distribution of the electric field are shown in Supplementary Figure 11. The exciton FRET rate, Γ_{X^0FRET}, is calculated by[44−46]

$$\Gamma_{X^0FRET} = \frac{2}{\hbar}\frac{\mathrm{Im}(\varepsilon_{MoSe2}(\omega_{exc}))}{4\pi}\int_{MoSe2} E\cdot E^* dV \quad (1)$$

where ε_{MoSe2} (ω_{exc}) is the $MoSe_2$ dielectric function at the exciton frequency of the WS_2, $\mathbf{E}$ is the electric field induced by an oscillating exciton dipole $\mu e^{-i\omega_{exc}t}$ (μ is dipole moment) and the integral is taken over the $MoSe_2$ layer. The in-plane dipole in WS_2 has a μ = 13 Debye, with other parameters shown in Supplementary Table 2.[11,47] Accordingly, the computed Γ_{X^0FRET} is $\Gamma_{X^0FRET} = 2.1 \times 10^{10}$ s^{-1}, corresponding to the FRET transfer time τ_{X^0FRET} = 47.6 ps. This value is significantly longer than WS_2 exciton lifetime (<13.8 ps) and trion formation lifetime (both lie in the range from subpicosecond to several picoseconds),[34,35,39−42] excluding the exciton as the donor of FRET. Similarly, we check the trion ET dynamics, as detailed in Supplementary Figure 12. The estimated trion energy transfer rate Γ_{x^-ET} is $\Gamma_{x^-ET} = 1.85 \times 10^{13}$ s^{-1}, corresponding to a transfer time of 0.054 ps, which is faster than the exciton FRET rate ($\Gamma_{x^0FRET} = 2.1 \times 10^{10}$ s^{-1}) and meantime shorter than the trion lifetime in WS_2 (57.4 ps). The Γ_{x^-ET} is faster than the value obtained experimentally (38.4 ps) because of the following reasons: (1) the trion lifetime in the heterojunction is close to the IRF, which may cause some overestimation of the lifetime, so as the underestimation of

https://dx.doi.org/10.1021/acsnano.0c05447
ACS Nano 2020, 14, 13470−13477

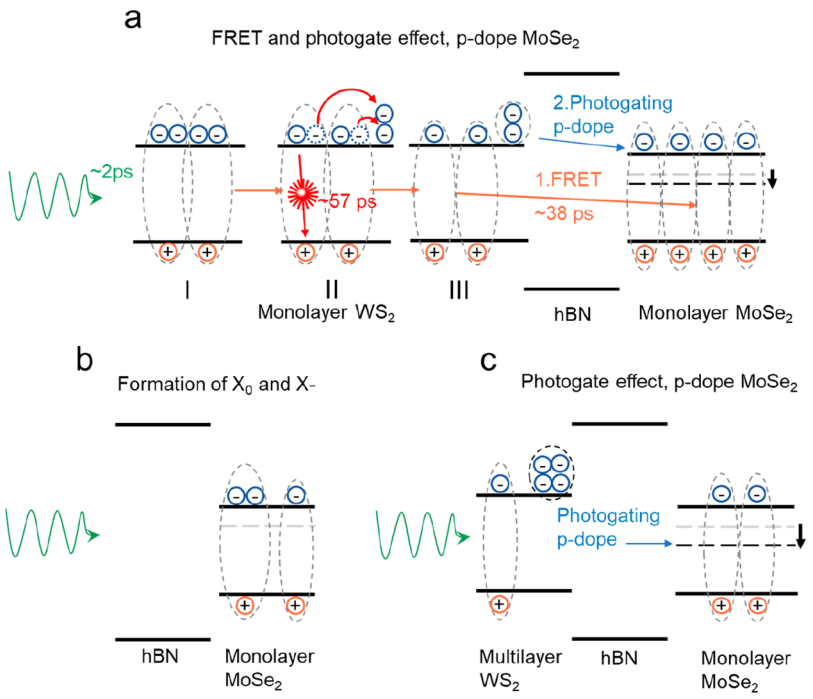

Figure 5. Schematic band diagrams and dynamic processes in different heterojunctions with the above WS_2 bandgap excitation. (a) Monolayer WS_2/hBN/monolayer $MoSe_2$, (b) hBN/monolayer $MoSe_2$, (c) multilayer WS_2/hBN/monolayer $MoSe_2$. The dashed line in $MoSe_2$ indicates the Fermi level.

FRET rate; (2) the formula 1 was developed to estimate the exciton FRET rate, which may need a coefficient of correction in the trion ET rate calculation. Further theoretical work is required to get a deeper understanding of the underlying physics.

Based on the preceding optical spectroscopy and transport measurements, we can conclude the realistic band alignment models for three different scenarios as shown in Figure 5. The dynamics in the monolayer WS_2/hBN/monolayer $MoSe_2$ heterojunction include three steps, that is, (I) the formation of trions in WS_2 within ~2 ps on optical pumping; (II) ~40.1% trions recombine via the recombination of electron−hole pair in the time scale of ~57 ps; (III) the tunneling of the dominant electron−hole pairs (~59.9%) into $MoSe_2$ via FRET in the time scale of ~38 ps (Figure 5a). The electrons generated in step (II) accumulate at the WS_2/hBN interface and serve as the photogate. In contrast, the laser excitation only induces excitons and trions in hBN/monolayer $MoSe_2$ (Figure 5b). In multilayer WS_2/hBN/monolayer $MoSe_2$, the optically generated electrons accumulate at the WS_2/hBN interface and gate the $MoSe_2$, leading to the exciton-dominated emission in the PL spectrum (Figure 5c).

CONCLUSIONS

In conclusion, we have demonstrated a clear picture of the energy transfer dynamics in 2D WS_2/hBN/$MoSe_2$ heterojunction. Specifically, the dynamics are mediated by the trions, in which ~59.9% electron−hole pairs from the trions transfer into $MoSe_2$ via FRET channels (τ_{FRET} ~ 38.4 ps) and the rest ~40.1% recombine by emitting photons in WS_2 (τ_{donor} ~ 38.4 ps), while the extra electrons accumulate at the WS_2/hBN interface to photogate $MoSe_2$. These results are experimentally revealed by both the steady-state and the time-resolved optical spectroscopy and further supported by the numerical simulations. This mechanism is different from the dipole−dipole interaction in the molecular system and also different from the direct exciton−exciton interaction in 2D TMD heterojunctions reported to date. The understanding of the underlying physics lays the foundation for engineering the interlayer energy transfer in the 2D limit and realizing FRET-based high-performance optoelectronic devices.[48]

METHODS

Sample Preparation. TMD samples are first exfoliated from bulk crystals (hq Graphene) to polydimethylsiloxane stamps and then transferred layer by layer on SiO_2 (300 nm)/Si substrate in a nitrogen-filled glovebox. A poly(methyl methacrylate) A4 (Microchem, USA) resist was spin-coated on the sample and then baked at 150 °C for 10 min. We then used a scanning electron microscope (JEOL 7001F) equipped with the nanometer pattern generation system to pattern electrodes. The exposed chip was immersed in *methyl isobutyl ketone*: isopropanol (3:1) mixed solution for 90 s to finalize developing. After developing, the sample was loaded into a thermal evaporator (Elite Engineering, Singapore) to deposit a Cr/Au film with a thickness of 5/50 nm. Subsequently, the chip was immersed in acetone for lift-off procedure, followed by rinsing with isopropanol and then drying with nitrogen gas. The sample was ready after a high vacuum (10^{-6} mbar) annealing at 200 °C for 2 h.

Optical Spectroscopy Measurement. (1) For the absorption measurement, we used a microspectrophotometer (Craic 20) to measure the small size sample, and it is capable of measuring the sample size down to 10 μm. The spectral range can be covered from 400 to 2100 nm. (2) PL and Raman spectroscopy mapping were conducted on a spectrometer with a 800 mm focal length (Horiba-JY Evolution) equipped with a liquid nitrogen-cooled CCD detector. Samples were put in a continuous-flow cryostat fixed on an xyz translation stage. The optical signals are collected by a 50× long work distance objective. All the measurements were carried out at a low temperature of 80 K with an excitation power ~10 μW. (3) The time-resolved photoluminescence spectroscopy measurement was performed with a home-built confocal micro-PL setup. Samples were also put in the cryostat operated at 80 K. A Ti:sapphire femtosecond laser with ~100 fs pulses at 80 MHz is used as the excitation source. The

https://dx.doi.org/10.1021/acsnano.0c05447
ACS Nano 2020, 14, 13470−13477

emission of the laser is frequency-doubled to output 400 nm pulses and is focused (50× objective lens, NA = 0.65) onto the sample. The time-resolved photoluminescence emission is first spectrally resolved with a spectrometer with a focal length of 320 mm (Horiba-JY iHR320), and photons after the exit slit of the spectrometer are detected with an avalanche detector connected to a time-correlated single-photon counting module (PicoHarp 300). The excitation power is ∼5 μW.

ASSOCIATED CONTENT

Supporting Information

The Supporting Information is available free of charge at https://pubs.acs.org/doi/10.1021/acsnano.0c05447.

Absorption, Raman, and PL spectra from different samples; *I*−*V* performance and fitting; PL lifetime fitting; details of numerical simulations (PDF)

AUTHOR INFORMATION

Corresponding Author

Qihua Xiong − *Division of Physics and Applied Physics, School of Physical and Mathematical Sciences, Nanyang Technological University, 637371, Singapore; State Key Laboratory of Low-Dimensional Quantum Physics, Department of Physics, Tsinghua University, Beijing 100084, China;* orcid.org/0000-0002-2555-4363; Email: qihua@ntu.edu.sg

Authors

Zehua Hu − *Division of Physics and Applied Physics, School of Physical and Mathematical Sciences, Nanyang Technological University, 637371, Singapore;* orcid.org/0000-0002-1185-2992

Pedro Ludwig Hernández-Martínez − *LUMINOUS! Center of Excellence for Semiconductor Lighting and Display, School of Electrical and Electronics Engineering, Nanyang Technological University, Singapore 639798 Singapore*

Xue Liu − *Division of Physics and Applied Physics, School of Physical and Mathematical Sciences, Nanyang Technological University, 637371, Singapore*

Mohamed-Raouf Amara − *Division of Physics and Applied Physics, School of Physical and Mathematical Sciences, Nanyang Technological University, 637371, Singapore*

Weijie Zhao − *Division of Physics and Applied Physics, School of Physical and Mathematical Sciences, Nanyang Technological University, 637371, Singapore*

Kenji Watanabe − *Research Center for Functional Materials, National Institute for Materials Science, Tsukuba 305-0044, Japan;* orcid.org/0000-0003-3701-8119

Takashi Taniguchi − *International Center for Materials Nanoarchitectonics, National Institute for Materials Science, Tsukuba 305-0044, Japan;* orcid.org/0000-0002-1467-3105

Hilmi Volkan Demir − *LUMINOUS! Center of Excellence for Semiconductor Lighting and Display, School of Electrical and Electronics Engineering, Nanyang Technological University, Singapore 639798 Singapore; Department of Physics, Department of Electrical and Electronics Engineering, UNAM-National Nanotechnology Research Center and Institute of Materials Science and Nanotechnology, Bilkent University, Ankara 06800, Turkey;* orcid.org/0000-0003-1793-112X

Complete contact information is available at: https://pubs.acs.org/10.1021/acsnano.0c05447

Author Contributions

Q.X. supervised the research. Z.H. conceived the idea. Z.H. and X.L. prepared the heterostructures. P.H.M. and H.V.D. performed the numerical simulation. Z.H., X.L., and M.R.A. performed the microspectroscopy experiments. K.W. and T.T. provided the h-BN bulk crystals. Z.H., X.L., and Q.X. analyzed the data. Z.H. wrote the manuscript with input from all authors.

Funding

Q.X. gratefully acknowledges the Singapore Ministry of Education Tier3 Programme "Geometrical Quantum Materials" (MOE2018-T3-1-002), AcRF Tier2 grant (MOE2017-T2-1-040), and Tier1 grant (RG 194/17). Q.X. also acknowledges strong support from Singapore National Research Foundation Competitive Research Programme "Integrated On-chip Planar Coherent Light Sources" (NRF-CRP-21-2018-0007), and National Research Foundation-Agence Nationale de la Recherche (NRF-ANR) Grant (NRF2017-NRF-ANR005 2DCHIRAL). K.W. and T.T. acknowledge support from the Elemental Strategy Initiative conducted by the MEXT, Japan, Grant Number JPMXP0112101001, JSPS KAKENHI Grant Numbers JP20H00354, and the CREST(JPMJCR15F3), JST.

Notes

The authors declare no competing financial interest.

REFERENCES

(1) Scholes, G. D. Long-Range Resonance Energy Transfer in Molecular Systems. *Annu. Rev. Phys. Chem.* **2003**, *54*, 57−87.

(2) Förster, T. Zwischenmolekulare energiewanderung und Fluoreszenz. *Ann. Phys.* **1948**, *437*, 55−75.

(3) Dexter, D. L. A Theory of Sensitized Luminescence in Solids. *J. Chem. Phys.* **1953**, *21*, 836−850.

(4) Lu, S.; Lingley, Z.; Asano, T.; Harris, D.; Barwicz, T.; Guha, S.; Madhukar, A. J. N. l. Photocurrent Induced by Nonradiative Energy Transfer from Nanocrystal Quantum Dots to Adjacent Silicon Nanowire Conducting Channels: Toward a New Solar Cell Paradigm. *Nano Lett.* **2009**, *9*, 4548−4552.

(5) Achermann, M.; Petruska, M. A.; Kos, S.; Smith, D. L.; Koleske, D. D.; Klimov, V. I. Energy-Transfer Pumping of Semiconductor Nanocrystals Using an Epitaxial Quantum Well. *Nature* **2004**, *429*, 642−646.

(6) Cerdán, L.; Enciso, E.; Martín, V.; Bañuelos, J.; López-Arbeloa, I.; Costela, A.; García-Moreno, I. FRET-Assisted Laser Emission in Colloidal Suspensions of Dye-Doped Latex Nanoparticles. *Nat. Photonics* **2012**, *6*, 621−626.

(7) Lyo, S. K. Energy Transfer from An Electron-Hole Plasma Layer to a Quantum Well in Semiconductor Structures. *Phys. Rev. B: Condens. Matter Mater. Phys.* **2010**, *81*, 115303.

(8) Martínez, P. L. H.; Govorov, A.; Demir, H. *Understanding and Modeling Föörster-Type Resonance Energy Transfer (FRET): FRET from Single Donor to Single Acceptor and Assemblies of Acceptors*; Springer: Singapore, 2017; Vol. 2, pp 18−21.

(9) Wang, Q. H.; Kalantar-Zadeh, K.; Kis, A.; Coleman, J. N.; Strano, M. S. Electronics and Optoelectronics of Two-Dimensional Transition Metal Dichalcogenides. *Nat. Nanotechnol.* **2012**, *7*, 699−712.

(10) Hu, Z.; Wu, Z.; Han, C.; He, J.; Ni, Z.; Chen, W. Two-Dimensional Transition Metal Dichalcogenides: Interface and Defect Engineering. *Chem. Soc. Rev.* **2018**, *47*, 3100−3128.

(11) Chernikov, A.; Berkelbach, T. C.; Hill, H. M.; Rigosi, A.; Li, Y.; Aslan, O. B.; Reichman, D. R.; Hybertsen, M. S.; Heinz, T. F. Exciton Binding Energy and Nonhydrogenic Rydberg Series in Monolayer WS_2. *Phys. Rev. Lett.* **2014**, *113*, 076802.

(12) You, Y.; Zhang, X.-X.; Berkelbach, T. C.; Hybertsen, M. S.; Reichman, D. R.; Heinz, T. F. Observation of Biexcitons in Monolayer WSe_2. *Nat. Phys.* **2015**, *11*, 477−481.

(13) Mak, K. F.; He, K.; Lee, C.; Lee, G. H.; Hone, J.; Heinz, T. F.; Shan, J. Tightly Bound Trions in Monolayer MoS_2. *Nat. Mater.* **2013**, *12*, 207−211.
(14) Xiao, D.; Liu, G. B.; Feng, W.; Xu, X.; Yao, W. Coupled Spin and Valley Physics in Monolayers of MoS_2 and Other Group-VI Dichalcogenides. *Phys. Rev. Lett.* **2012**, *108*, 196802.
(15) Schaibley, J. R.; Yu, H.; Clark, G.; Rivera, P.; Ross, J. S.; Seyler, K. L.; Yao, W.; Xu, X. Valleytronics in 2D Materials. *Nat. Rev. Mater.* **2016**, *1*, 1−15.
(16) Hong, X.; Kim, J.; Shi, S. F.; Zhang, Y.; Jin, C.; Sun, Y.; Tongay, S.; Wu, J.; Zhang, Y.; Wang, F. Ultrafast Charge Transfer in Atomically Thin MoS_2/WS_2 Heterostructures. *Nat. Nanotechnol.* **2014**, *9*, 682−686.
(17) Xu, W.; Liu, W.; Schmidt, J. F.; Zhao, W.; Lu, X.; Raab, T.; Diederichs, C.; Gao, W.; Seletskiy, D. V.; Xiong, Q. Correlated Fluorescence Blinking in Two-Dimensional Semiconductor Heterostructures. *Nature* **2017**, *541*, 62−67.
(18) Kim, J.; Jin, C.; Chen, B.; Cai, H.; Zhao, T.; Lee, P.; Kahn, S.; Watanabe, K.; Taniguchi, T.; Tongay, S.; Crommie, M. F.; Wang, F. Observation of Ultralong Valley Lifetime in WSe_2/MoS_2 Heterostructures. *Sci. Adv.* **2017**, *3*, No. e1700518.
(19) Du, W.; Zhao, J.; Zhao, W.; Zhang, S.; Xu, H.; Xiong, Q. Ultrafast Modulation of Exciton−Plasmon Coupling in a Monolayer WS_2−Ag Nanodisk Hybrid System. *ACS Photonics* **2019**, *6*, 2832−2840.
(20) Wen, X.; Xu, W.; Zhao, W.; Khurgin, J. B.; Xiong, Q. Plasmonic Hot Carriers-Controlled Second Harmonic Generation in WSe_2 Bilayers. *Nano Lett.* **2018**, *18*, 1686−1692.
(21) Long, R.; Prezhdo, O. V. Quantum Coherence Facilitates Efficient Charge Separation at a MoS_2/$MoSe_2$ van der Waals Junction. *Nano Lett.* **2016**, *16*, 1996−2003.
(22) Rivera, P.; Schaibley, J. R.; Jones, A. M.; Ross, J. S.; Wu, S.; Aivazian, G.; Klement, P.; Seyler, K.; Clark, G.; Ghimire, N. J.; Yan, J.; Mandrus, D. G.; Yao, W.; Xu, X. Observation of Long-Lived Interlayer Excitons in Monolayer $MoSe_2$-WSe_2 Heterostructures. *Nat. Commun.* **2015**, *6*, 6242.
(23) Rivera, P.; Seyler, K. L.; Yu, H.; Schaibley, J. R.; Yan, J.; Mandrus, D. G.; Yao, W.; Xu, X. Valley-Polarized Exciton Dynamics in a 2D semiconductor Heterostructure. *Science* **2016**, *351*, 688−691.
(24) Zang, H.; Routh, P. K.; Huang, Y.; Chen, J. S.; Sutter, E.; Sutter, P.; Cotlet, M. Nonradiative Energy Transfer from Individual CdSe/ZnS Quantum Dots to Single-Layer and Few-Layer Tin Disulfide. *ACS Nano* **2016**, *10*, 4790−4796.
(25) Raja, A.; Montoya Castillo, A.; Zultak, J.; Zhang, X. X.; Ye, Z.; Roquelet, C.; Chenet, D. A.; van der Zande, A. M.; Huang, P.; Jockusch, S.; Hone, J.; Reichman, D. R.; Brus, L. E.; Heinz, T. F. Energy Transfer from Quantum Dots to Graphene and MoS_2: The Role of Absorption and Screening in Two-Dimensional Materials. *Nano Lett.* **2016**, *16*, 2328−2333.
(26) Prins, F.; Goodman, A. J.; Tisdale, W. A. Reduced Dielectric Screening and Enhanced Energy Transfer in Single- and Few-layer MoS_2. *Nano Lett.* **2014**, *14*, 6087−6091.
(27) Liu, Y.; Li, H.; Zheng, X.; Cheng, X.; Jiang, T. Giant Photoluminescence Enhancement in Monolayer WS_2 by Energy Transfer from CsPbBr3 Quantum Dots. *Opt. Mater. Express* **2017**, *7*, 1327.
(28) Zhang, L.; Sharma, A.; Zhu, Y.; Zhang, Y.; Wang, B.; Dong, M.; Nguyen, H. T.; Wang, Z.; Wen, B.; Cao, Y.; Liu, B.; Sun, X.; Yang, J.; Li, Z.; Kar, A.; Shi, Y.; Macdonald, D.; Yu, Z.; Wang, X.; Lu, Y. Efficient and Layer-Dependent Exciton Pumping across Atomically Thin Organic-Inorganic Type-I Heterostructures. *Adv. Mater.* **2018**, *30*, No. 1803986.
(29) Froehlicher, G.; Lorchat, E.; Berciaud, S. Charge Versus Energy Transfer in Atomically Thin Graphene-Transition Metal Dichalcogenide van der Waals Heterostructures. *Phys. Rev. X* **2018**, *8*, 011007.
(30) Liu, X.; Pei, J.; Hu, Z.; Zhao, W.; Liu, S.; Amara, M. R.; Watanabe, K.; Taniguchi, T.; Zhang, H.; Xiong, Q. Manipulating Charge and Energy Transfer between 2D Atomic Layers via Heterostructure Engineering. *Nano Lett.* **2020**, *20*, 5359−5366.
(31) Kozawa, D.; Carvalho, A.; Verzhbitskiy, I.; Giustiniano, F.; Miyauchi, Y.; Mouri, S.; Castro Neto, A. H.; Matsuda, K.; Eda, G. Evidence for Fast Interlayer Energy Transfer in $MoSe_2$/WS_2 Heterostructures. *Nano Lett.* **2016**, *16*, 4087−4093.
(32) Wu, L.; Chen, Y.; Zhou, H.; Zhu, H. Ultrafast Energy Transfer of Both Bright and Dark Excitons in 2D van der Waals Heterostructures Beyond Dipolar Coupling. *ACS Nano* **2019**, *13*, 2341−2348.
(33) Xu, W.; Kozawa, D.; Liu, Y.; Sheng, Y.; Wei, K.; Koman, V. B.; Wang, S.; Wang, X.; Jiang, T.; Strano, M. S.; Warner, J. H. Determining the Optimized Interlayer Separation Distance in Vertical Stacked 2D WS_2: hBN: MoS_2 Heterostructures for Exciton Energy Transfer. *Small* **2018**, *14*, No. 1703727.
(34) Zhao, J.; Zhao, W.; Du, W.; Su, R.; Xiong, Q. Dynamics of Exciton Energy Renormalization in Monolayer Transition Metal Disulfides. *Nano Res.* **2020**, *13*, 1399.
(35) Robert, C.; Lagarde, D.; Cadiz, F.; Wang, G.; Lassagne, B.; Amand, T.; Balocchi, A.; Renucci, P.; Tongay, S.; Urbaszek, B.; Marie, X. Exciton Radiative Lifetime in Transition Metal Dichalcogenide Monolayers. *Phys. Rev. B: Condens. Matter Mater. Phys.* **2016**, *93*, 205423.
(36) Chakraborty, B.; Bera, A.; Muthu, D. V. S.; Bhowmick, S.; Waghmare, U. V.; Sood, A. K. Symmetry-Dependent Phonon Renormalization in Monolayer MoS_2 Transistor. *Phys. Rev. B: Condens. Matter Mater. Phys.* **2012**, *85*, 161403.
(37) Stavola, M.; Dexter, D. L.; Knox, R. S. Electron-Hole Pair Excitation in Semiconductors via Energy Transfer from An External Sensitizer. *Phys. Rev. B: Condens. Matter Mater. Phys.* **1985**, *31*, 2277−2289.
(38) Kang, J.; Tongay, S.; Zhou, J.; Li, J.; Wu, J. Band Offsets and Heterostructures of Two-Dimensional Semiconductors. *Appl. Phys. Lett.* **2013**, *102*, 012111.
(39) Wang, H.; Zhang, C.; Chan, W.; Manolatou, C.; Tiwari, S.; Rana, F. Radiative Lifetimes of Excitons and Trions in Monolayers of the Metal Dichalcogenide MoS_2. *Phys. Rev. B: Condens. Matter Mater. Phys.* **2016**, *93*, 045407.
(40) Palummo, M.; Bernardi, M.; Grossman, J. C. Exciton Radiative Lifetimes in Two-Dimensional Transition Metal Dichalcogenides. *Nano Lett.* **2015**, *15*, 2794−2800.
(41) Poellmann, C.; Steinleitner, P.; Leierseder, U.; Nagler, P.; Plechinger, G.; Porer, M.; Bratschitsch, R.; Schuller, C.; Korn, T.; Huber, R. Resonant Internal Quantum Transitions and Femtosecond Radiative Decay of Excitons in Monolayer WSe_2. *Nat. Mater.* **2015**, *14*, 889−893.
(42) Singh, A.; Moody, G.; Tran, K.; Scott, M. E.; Overbeck, V.; Berghäuser, G.; Schaibley, J.; Seifert, E. J.; Pleskot, D.; Gabor, N. M.; Yan, J.; Mandrus, D. G.; Richter, M.; Malic, E.; Xu, X.; Li, X. Trion Formation Dynamics in Monolayer Transition Metal Dichalcogenides. *Phys. Rev. B: Condens. Matter Mater. Phys.* **2016**, *93*, 041401.
(43) Sampat, S.; Guo, T.; Zhang, K.; Robinson, J. A.; Ghosh, Y.; Acharya, K. P.; Htoon, H.; Hollingsworth, J. A.; Gartstein, Y. N.; Malko, A. V. Exciton and Trion Energy Transfer from Giant Semiconductor Nanocrystals to MoS_2 Monolayers. *ACS Photonics* **2016**, *3*, 708−715.
(44) Govorov, A. O.; Carmeli, I. Hybrid Structures Composed of Photosynthetic System and Metal Nanoparticles: Plasmon Enhancement Effect. *Nano Lett.* **2007**, *7*, 620−625.
(45) Hernández-Martínez, P. L.; Govorov, A. O. Exciton Energy Transfer between Nanoparticles and Nanowires. *Phys. Rev. B: Condens. Matter Mater. Phys.* **2008**, *78*, 035314.
(46) Hernández-Martínez, P. L.; Govorov, A. O.; Demir, H. V. Generalized Theory of Forster-Type Nonradiative Energy Transfer in Nanostructures with Mixed Dimensionality. *J. Phys. Chem. C* **2013**, *117*, 10203−10212.
(47) Feierabend, M.; Berghäuser, G.; Selig, M.; Brem, S.; Shegai, T.; Eigler, S.; Malic, E. Molecule Signatures in Photoluminescence Spectra of Transition Metal Dichalcogenides. *Phys. Rev. Mater.* **2018**, *2*, 014004.

https://dx.doi.org/10.1021/acsnano.0c05447
ACS Nano 2020, 14, 13470−13477

(48) Kim, J.; Kim, H.-R.; Lee, H.-C.; Kim, K.-H.; Hwang, M.-S.; Lee, J. M.; Jeong, K.-Y.; Park, H.-G. Photon-Triggered Current Generation in Chemically-Synthesized Silicon Nanowires. *Nano Lett.* **2019**, *19*, 1269−1274.

https://dx.doi.org/10.1021/acsnano.0c05447
ACS Nano 2020, 14, 13470−13477